Medical Engineering & Physics 36 (2014) 592–600

Contents lists available at ScienceDirect

Medical Engineering & Physics

journal homepage: www.elsevier.com/locate/medengphy

Nonstationary multivariate modeling of cerebral autoregulation during hypercapnia

Kyriaki Kostoglou[a], Chantel T. Debert[b], Marc J. Poulin[c,d,e,f,g], Georgios D. Mitsis[a,*]

[a] Department of Electrical and Computer Engineering, University of Cyprus, Nicosia, Cyprus
[b] Department of Physical Medicine and Rehabilitation, Faculty of Medicine, University of Calgary, AB, Canada
[c] Department of Physiology & Pharmacology, Faculty of Medicine, University of Calgary, AB, Canada
[d] Department of Clinical Neurosciences, Faculty of Medicine, University of Calgary, AB, Canada
[e] Faculty of Kinesiology, University of Calgary, AB, Canada
[f] Hotchkiss Brain Institute, Faculty of Medicine, University of Calgary, AB, Canada
[g] Libin Cardiovascular Institute of Alberta, Faculty of Medicine, University of Calgary, AB, Canada

ARTICLE INFO

Article history:
Received 5 March 2013
Received in revised form 7 September 2013
Accepted 13 October 2013

Keywords:
Cerebral hemodynamics
Time varying systems
CO_2 reactivity
Laguerre functions
Recursive Least Squares
Multiple forgetting factors

ABSTRACT

We examined the time-varying characteristics of cerebral autoregulation and hemodynamics during a step hypercapnic stimulus by using recursively estimated multivariate (two-input) models which quantify the dynamic effects of mean arterial blood pressure (ABP) and end-tidal CO_2 tension (P_{ETCO_2}) on middle cerebral artery blood flow velocity (CBFV). Beat-to-beat values of ABP and CBFV, as well as breath-to-breath values of P_{ETCO_2} during baseline and sustained euoxic hypercapnia were obtained in 8 female subjects. The multiple-input, single-output models used were based on the Laguerre expansion technique, and their parameters were updated using recursive least squares with multiple forgetting factors. The results reveal the presence of nonstationarities that confirm previously reported effects of hypercapnia on autoregulation, i.e. a decrease in the MABP phase lead, and suggest that the incorporation of P_{ETCO_2} as an additional model input yields less time-varying estimates of dynamic pressure autoregulation obtained from single-input (ABP–CBFV) models.

© 2013 IPEM. Published by Elsevier Ltd. All rights reserved.

1. Introduction

Cerebral autoregulation collectively refers to the ability of the cerebrovascular bed to maintain a relatively constant cerebral blood flow (CBF) in response to variations in several physiological variables. The most important of these variables is arterial blood pressure (ABP); therefore, the relation between ABP and CBF is typically used to characterize autoregulation. Accurate quantitative assessment of cerebral autoregulation and, more generally, hemodynamics, is important in the context of cerebrovascular disease diagnosis and monitoring [1,2]. Following the advance of transcranial Doppler ultrasound (TCD), which yields accurate measurements of CBF velocity (CBFV) [3], it is now well established that autoregulation is a dynamic, frequency-dependent phenomenon [4–6]. Dynamic autoregulation may be assessed from the CBFV response to step-like, externally induced ABP stimuli or from spontaneous physiological variability, as the latter exhibits sufficiently broadband characteristics. The majority of the studies that have assessed dynamic cerebral autoregulation from spontaneous variability have utilized univariate, linear techniques such as transfer function analysis [4]. However, in this latter study and other studies, low coherence values (<0.5) between spontaneous ABP and CBFV fluctuations in the frequency range below 0.07 Hz have been reported. Since coherence is a measure of linearity in the dynamic relation between ABP and CBFV, this suggests that nonlinearities and/or other physiological variables may have an important effect in this frequency range. In this context, it is well known that the cerebral vasculature is extremely sensitive to arterial CO_2 changes; for instance, spontaneous variations of end-tidal CO_2 (P_{ETCO_2}) have been shown to influence CBFV as well as the BOLD fMRI signal [7,8]. Therefore, multivariate models of cerebral hemodynamics incorporating CO_2 as an additional input have been proposed in order to characterize autoregulation [7,9]. The presence of nonlinearities has been also suggested [5,6], corroborating that the aforementioned low coherence between ABP and CBFV is due to both factors. In our previous studies, we have demonstrated that both dynamic nonlinearities and CO_2 variability account for a significant fraction of the low-frequency CBFV variability during resting conditions, orthostatic stress as well as ganglion blockade [7,10,11]. Collectively, these findings suggest that multivariate and/or nonlinear modeling approaches yield more accurate quantitative descriptions of cerebral hemodynamics below 0.07 Hz.

* Corresponding author.
E-mail address: mitsis.georgios@ucy.ac.cy (G.D. Mitsis).

1350-4533/$ – see front matter © 2013 IPEM. Published by Elsevier Ltd. All rights reserved.
http://dx.doi.org/10.1016/j.medengphy.2013.10.011

Furthermore, an important property of the obtained dynamic cerebral autoregulation models, which is often ignored, is the possible presence of nonstationary (time-varying) characteristics. Such characteristics may influence the results considerably and should possibly be taken into account in order to obtain more reliable quantitative indices of dynamic autoregulation, e.g. for clinical purposes. Nonstationarities are often observed in physiological systems, due to the complexity of such systems and the effect of several unobservable physiological variables and/or physiological cycles that act in widely different time scales (e.g., local mechanisms may act within seconds, whereas diurnal or circadian mechanisms have a cycle on the order of several hours). Previous studies have suggested the presence of nonstationarities in cerebral autoregulation and hemodynamics using approaches both in the time and frequency domain, e.g. the autoregulatory index, nonlinear Volterra models, wavelets, as well as recursive estimation of parametric models [7,10–14,29,30].

Therefore, in the present paper, we employ a recursive scheme to estimate multivariate dynamic models, which is based on Laguerre function expansions, in order to obtain adaptive two-input models of cerebral hemodynamics (inputs: MABP and P_{ETCO_2}, output: CBFV) and quantify their nonstationary characteristics during a hypercapnic experimental protocol in young (pre-menopausal) female subjects. The experimental data are part of a larger set that includes postmenopausal women receiving hormonal therapy and not receiving therapy; however, here we focus on the time-varying characteristics of hemodynamics in young subjects as well as on the influence of the rapid transient changes induced by the hypercapnic step on these characteristics. Furthermore, the usefulness of gender-specific studies related to cerebral hemodynamics has been suggested, as the effect of gender and hormonal levels on vascular function as well as gender-related differences in cerebrovascular reactivity have been reported [16,17]. The results extend our recent findings regarding the presence of nonstationarities during resting conditions [18] and suggest that the relationship between MABP and CBFV is influenced by the addition of P_{ETCO_2}, as incorporating the latter as a model input yields less time-varying estimates of dynamic pressure autoregulation.

2. Methods

2.1. Experimental data

The experimental data were collected at the University of Calgary from 8 pre-menopausal (27.0 ± 7.1 yrs (mean ± SD)) women, who were tested in the follicular phase of the menstrual cycle. None of the subjects were taking medication, all were nonsmokers, and none had a history of cardiovascular, cerebrovascular, or respiratory disease. The subjects gave informed consent to participate in this study, which was approved by the University of Calgary Conjoint Health Research Ethics Board.

Each subject was positioned semi-supine and TCD was used to obtain CBFV measurements from the right middle cerebral artery (MCA) using a 2-MHz pulsed Doppler ultrasound system (TC22, SciMed, Bristol, UK). The MCA was identified using an insonation pathway through the right temporal window just above the zygomatic arch. The Doppler system was adapted to output signals associated with the maximum and intensity-weighted mean frequency shifts, which were updated each time a new spectrum was calculated (every 10 ms). For each 10-ms sample, the value for the blood velocity associated with the maximum frequency of the Doppler shift was calculated and recorded.

After taking resting measurements of end-tidal P_{CO_2} (P_{ETCO_2}) and P_{O_2} (P_{ETO_2}) for approximately 10 min, dynamic end-tidal forcing was used to control both arterial gas tensions. The protocol, shown in Fig. 1a for a representative subject, consisted of a 10 min period, when mean P_{ETO_2} was held constant at 88 mmHg and mean P_{ETCO_2} was held 1.0 mmHg above the subject's natural resting value, followed by 20 min of hypercapnia, when mean P_{ETCO_2} was held 8 mmHg above resting levels and a 10 min period when mean P_{ETCO_2} was held to its prehypercapnic value. ABP was monitored with finger photoplethysmography (Portapress, TPD Biomedical Instrumentation, The Netherlands).

Beat-to-beat mean values of ABP (MABP) and CBFV were calculated by integrating the waveform of the sampled signals within each cardiac cycle. The beat-to-beat values of MABP and CBFV and the breath-to-breath values of P_{ETCO_2} were then interpolated and resampled at 1 Hz to obtain equally spaced time series data (Fig. 1a). Pure time delay for the P_{ETCO_2} effects was taken into account and the P_{ETCO_2} time-series were shifted accordingly when performing model estimation. Boxplots for the steady-state values of CBFV, MABP and P_{ETCO_2} are shown in Fig. 1b. All hemodynamic signals increased during hypercapnia, with the increase in P_{ETCO_2} being significant and the increase in CBFV being marginally significant (analysis of variance – ANOVA – with Fisher's least significance difference procedure for post hoc comparisons). CBFV and P_{ETCO_2} decreased significantly post-hypercapnia compared to hypercapnia, while the corresponding changes in MABP were not significant.

2.2. Mathematical methods

2.2.1. Two input discrete-time model

The input–output relationship of a linear, two-input, single-output, causal and dynamic system can be written in discrete-time as follows [19]:

$$y(n) = k0 + \sum_{i=1}^{2}\sum_{m} k_1^{(x_i)}(m)x_i(n-m) \tag{1}$$

where $x_1(n)$ and $x_2(n)$ are the two inputs (MABP and P_{ETCO_2} respectively), $y(n)$ is the output (CBFV) and $k_1^{(x_i)}$ are the impulse responses associated with the two model inputs. Eq. (1) is a special case of the multiple-input Volterra models, whereby $k_1^{(x_i)}$ are the first-order (linear) Volterra kernels of the system. The zero-order term k_0 is the output of the system when all inputs are absent. An efficient way to estimate the linear kernels is the Laguerre expansion technique (LET) [20]. Specifically, the discretized kernels can be expanded in terms of the orthonormal basis of discrete-time Laguerre functions (DLFs) as follows:

$$k_1^{(x_i)}(m) = \sum_{j=0}^{L_{x_i}-1} c_j^{(x_i)}(j) b_j^{(x_i)}(m) \tag{2}$$

where $i = 1, 2$ and $b_j^{(x_i)}(m)$ is the j-th order discrete time Laguerre function corresponding to input i:

$$b_j^{(x_i)}(m) = a_i^{(m-j)/2}(1-a_i)^{1/2}\sum_{k=0}^{j}(-1)^k \binom{m}{k}\binom{j}{k} a_i^{j-k}(1-a_i)^k \tag{3}$$

The expansion coefficients $c_j^{(x_i)}$ can be estimated using least-squares estimation based on the input and output data [20]. The parameters a_i lie between 0 and 1 and determine the rate of exponential decay of the DLFs; here, we use a different parameter for each input, as different inputs are typically characterized by different dynamic characteristics, as is the case in the present application (MABP explains most of the high-frequency CBFV variability, while P_{ETCO_2} explains a significant fraction of low-frequency CBFV variability [7]). Choosing an appropriate value for these parameters is important as it affects model accuracy and complexity and we

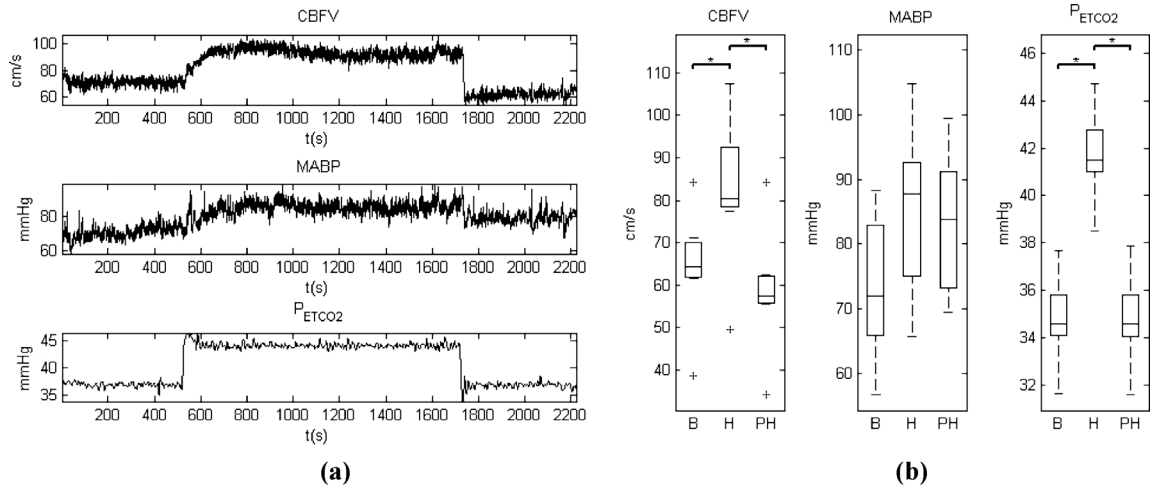

Fig. 1. (a) Representative segments of experimental data from one subject and (b) boxplots of the mean values of the hemodynamic signals over all subjects during baseline (B), hypercapnia (H) and post-hypercapnia (PH). One-way analysis of variance (ANOVA) and post hoc comparisons were used: $^{*}p < 0.05$.

describe below the procedure that we followed. Since the initial values of the Laguerre functions are non-zero, shifting the P_{ETCO_2} time series is recommended in order to deal with the pure time delay of the P_{ETCO_2} effects. By combining Eqs. (1) and (2) we can write:

$$\boldsymbol{y} = \boldsymbol{V}\boldsymbol{c} + \varepsilon \tag{4}$$

where $\boldsymbol{y}$ is the output vector (CBFV), $\boldsymbol{V}$ is a matrix containing the convolution of both inputs with the Laguerre functions and $\boldsymbol{c}$ is the vector of the unknown expansion coefficients. The number of free parameters is equal to $1 + L_{x_{i_1}} + L_{x_{i_2}}$ and the two linear kernels quantify the dynamic effects of MABP (dynamic pressure autoregulation) and P_{ETCO_2} (dynamic CO_2 reactivity) on CBFV, respectively.

2.2.2. Recursive least squares with multiple forgetting factors

In order to estimate and track the parameters of a time-varying system, the Recursive Least Squares (RLS) algorithm with forgetting factor is commonly used [21]. In the present study, since the two inputs have been shown to exhibit different dynamics [7], suggesting that the corresponding model parameters may vary with different rates, a multiple adaptive forgetting factor scheme has been applied [21–24]. The update equations for the unknown coefficients vector ($\hat{\boldsymbol{c}}$) at time point t are written as:

$$e(t) = y(t) - \boldsymbol{v}^T(t)\hat{\boldsymbol{c}}(t-1) \tag{5}$$

$$r(t) = \boldsymbol{v}^T(t)\boldsymbol{P}(t-1)\boldsymbol{v}(t) \tag{6}$$

$$\boldsymbol{K}(t) = \frac{\boldsymbol{P}(t-1)\boldsymbol{v}(t)}{1 + r(t)} \tag{7}$$

$$\hat{\boldsymbol{c}}(t) = \hat{\boldsymbol{c}}(t-1) + \boldsymbol{K}(t)e(t) \tag{8}$$

$$\boldsymbol{W}(t) = \boldsymbol{P}(t-1) - \frac{\boldsymbol{P}(t-1)\boldsymbol{v}(t)\boldsymbol{v}^T(t)\boldsymbol{P}(t-1)}{1 + r(t)} \tag{9}$$

$$\boldsymbol{P}(t) = \boldsymbol{\Lambda}(t)\boldsymbol{W}(t)\boldsymbol{\Lambda}(t) \quad (\in \mathbf{R}^{n\times n}, n = 1 + L_{x_{i_1}} + L_{x_{i_2}}) \tag{10}$$

$$\boldsymbol{\Lambda}(t) = diag\left(\sqrt{\frac{1}{\lambda_i(t)}}\right) \quad (i = 1, 2, \ldots, n) \tag{11}$$

where $e(t)$ is the output prediction error, $\boldsymbol{v}(t)$ is the row of the matrix $\boldsymbol{V}$ corresponding to time t, $\boldsymbol{K}(t)$ is the gain matrix and $\boldsymbol{P}(t)$ is the covariance matrix of the coefficient estimates. The parameters λ_i are the so called forgetting factors and lie between 0 and 1. Their role is to give exponentially less weight to less recent error samples and adapt the size of the matrix $\boldsymbol{P}(t)$ in order to track the time varying parameters of the system.

To account for the different dynamics associated with each input, three distinct forgetting factors were used. The first corresponds to the zero-order kernel coefficient and the remaining two correspond to the first-order kernel coefficients for MABP and P_{ETCO_2} respectively. The forgetting factors may be treated as constant or adaptive, i.e. dependent on time t; one way to compute them adaptively is by measuring the influence of the new data using Cook's distance and translating it into forgetting factors [23]. Adaptive data-driven forgetting factors were found to yield better performance, since the resulting parameter estimates were found to be less variable; hence we present results for this case.

2.3. Model order selection

The model order complexity L_{x_i} for each input, the values for a_i, i.e. the parameters that determine the exponential decay of the Laguerre functions, the limits of the forgetting factors (λ_{min}, λ_{max}) and the pure time delay for the P_{ETCO_2} effects (d seconds) were optimized with the help of a mixed integer Genetic Algorithm (GA). Genetic algorithms are adaptive search algorithms based on the idea of natural evolution. A population of candidate solutions, called individuals, evolves toward better solutions. In each generation, the fitness functions of every individual in the population are evaluated and the fitter individuals are selected randomly to form a new population that will be used in the next iteration of the algorithm. The algorithm is terminated if a maximum number of iterations or a fitness level has been reached. The fitness function selected to be minimized was the exponential of the negative output prediction Variance Accounted For (enVAF) for the entire dataset,

$$enVAF(n) = e^{-(1-(\sigma_e^2/\sigma_y^2))}, \quad \text{where } VAF(n) = 1 - \frac{\sigma_e^2}{\sigma_y^2}$$

where $\boldsymbol{e} = \boldsymbol{y} - \hat{\boldsymbol{y}}$ is the output prediction error, $\boldsymbol{y}$ is the actual and $\hat{\boldsymbol{y}}$ the predicted output.

For the adaptive forgetting factors case candidate solutions for a one-input and a two-input linear system are of the form,

$$[L_1, a_1, \lambda_{min_1}, \lambda_{max_1}] \text{ and } [L_1, L_2, a_1, a_2, \lambda_{min_1}, \lambda_{min_2}, \lambda_{max_1}, \lambda_{max_2}, d]$$

where subscripts 1 and 2 correspond to the MABP and the P_{ETCO_2} input, respectively. For the one-input model since

Table 1
Model parameters (fitness function used: enVAF). Subscripts 0, 1 and 2 correspond to the zero-order kernel, the MABP and P_{ETCO_2} input, respectively. (a) One-input model without a zero-order term; overfitting is evident; (b) one-input model with zero-order term; distinct forgetting factors are used for the zero-order kernel and the MABP input. (c) Two-input model using full covariance matrix $\boldsymbol{P}$; (d) two-input model using a diagonal covariance matrix $\boldsymbol{P}$. The lower and upper bounds were set to [1, 30] for the number of Laguerre functions (L), [0.1, 0.99] for the Laguerre parameters (a), [0.1, 0.999] for the limits of the forgetting factors and [1, 10] s for the pure time delay of the P_{ETCO_2} time series.

(a)

Subject	L_1	a_1	λ_{min_1}	λ_{max_1}	VAF (%)
1	30	0.792	0.859	0.985	97.749
2	7	0.776	0.310	0.874	97.456
3	24	0.773	0.314	0.977	98.253
4	18	0.826	0.567	0.971	94.601
5	25	0.779	0.544	0.978	91.223
6	19	0.727	0.389	0.965	98.057
7	8	0.806	0.866	0.930	93.977
8	30	0.782	0.225	0.982	95.176

(b)

Subject	L_1	a_1	λ_{min_0}	λ_{max_0}	λ_{min_1}	λ_{max_1}	VAF (%)
1	8	0.100	0.111	0.824	0.979	0.981	98.109
2	7	0.561	0.130	0.526	0.962	0.977	98.110
3	8	0.147	0.122	0.755	0.820	0.977	98.404
4	4	0.100	0.224	0.492	0.773	0.985	96.120
5	4	0.153	0.321	0.527	0.748	0.982	93.228
6	6	0.122	0.103	0.407	0.850	0.982	98.361
7	6	0.323	0.104	0.478	0.244	0.989	95.166
8	4	0.100	0.316	0.686	0.709	0.979	96.217

(c)

Subject	L_1	a_1	λ_{min_1}	λ_{max_1}	L_2	a_2	λ_{min_2}	λ_{max_2}	d (s)	VAF (%)
1	5	0.124	0.701	0.993	2	0.711	0.369	0.732	4	98.179
2	5	0.100	0.296	0.994	2	0.595	0.192	0.503	7	98.224
3	6	0.136	0.380	0.990	2	0.756	0.459	0.644	4	98.686
4	4	0.100	0.112	0.995	2	0.724	0.100	0.545	3	96.321
5	4	0.181	0.632	0.997	2	0.768	0.395	0.639	1	93.470
6	4	0.157	0.107	0.996	2	0.777	0.131	0.597	2	98.615
7	4	0.142	0.915	0.992	2	0.780	0.101	0.533	1	95.469
8	4	0.121	0.321	0.988	2	0.681	0.253	0.650	7	96.617

(d)

Subject	L_1	a_1	λ_{min_1}	λ_{max_1}	L_2	a_2	λ_{min_2}	λ_{max_2}	d (s)	VAF (%)
1	5	0.100	0.979	0.979	4	0.590	0.140	0.925	1	98.164
2	7	0.344	0.392	0.986	4	0.440	0.459	0.848	2	98.221
3	8	0.159	0.642	0.987	4	0.513	0.448	0.904	2	98.698
4	8	0.414	0.993	0.988	8	0.106	0.517	0.949	5	96.370
5	6	0.100	0.940	0.993	6	0.250	0.121	0.908	1	93.720
6	7	0.401	0.906	0.977	9	0.110	0.297	0.958	3	98.618
7	6	0.305	0.221	0.991	8	0.155	0.474	0.933	5	95.525
8	6	0.165	0.236	0.975	8	0.261	0.106	0.964	1	96.495

the effects of the hypercapnic step on the CBFV cannot be explained adequately by MABP, in order to avoid overfitting (Table 1), a forgetting factor is included for the zero-order term ($[L_1, a_1, \lambda_{min_0}, \lambda_{min_1}, \lambda_{max_0}, \lambda_{max_1}]$). For each candidate solution the procedure can be summarized as follows:

- Shift the P_{ETCO_2} time-series d points in time.
- Compute the $\boldsymbol{V}$ matrix using the recursive equations based on the selected L's and a's.
- Obtain the time-varying estimates $\hat{\boldsymbol{c}}$ using the algorithm described in equations (5)–(10).
- Compute the predicted output $\hat{\boldsymbol{y}} = \boldsymbol{V}\hat{\boldsymbol{c}}$.
- Estimate the error between the actual and the predicted output, $\boldsymbol{e} = \boldsymbol{y} - \hat{\boldsymbol{y}}$.
- Evaluate the fitness function selected for the entire training dataset.
- The solution that returns the lowest enVAF is selected for further analysis.

The final results for the one-input and the two-input models are presented in Table 1. At this point it has to be mentioned that since the system is nonstationary due to the presence of the hypercapnic step, using enVAF on the training dataset without a separate testing dataset did not lead to overfitting, as very complex models were found to be unable to adequately track the system nonstationarities. Additional model order selection criteria such as the Bayesian (BIC) and Akaike Information Criterion (AIC) were also examined and the results obtained were similar to those using enVAF (not shown here).

2.4. Nonstanionarities

In order to quantify the nonstationarities of the model estimates, the following variability index was computed for each extracted time-varying kernel [18],

$$VI_{x_i}(f) = 1/(N-1)\frac{\Sigma_{t=1}^{N}(p_t(f) - \bar{p}(f))^2}{\bar{p}(f)}$$

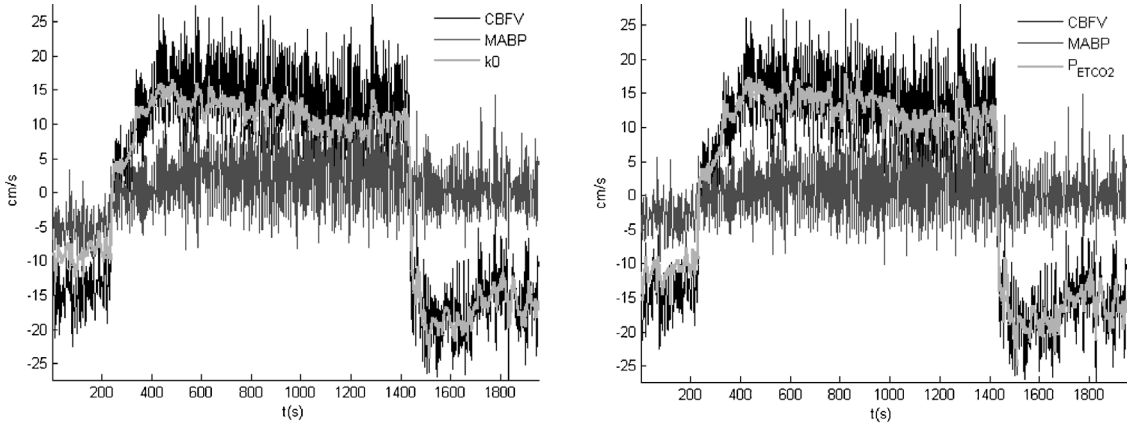

Fig. 2. Representative contributions of the inputs to the output prediction for: (a) one-input model (input: MABP, output: CBFV) and (b) two-input model (inputs: MABP, P_{ETCO_2}, output: CBFV) along with experimental CBFV measurements. Note that for the one input model the adaptive constant model term accounts for a significant fraction of CBFV variability that is due to P_{ETCO_2} (e.g. the increase caused by the hypercapnic step), which is not incorporated in the model.

where $p_t(f)$ is the FFT magnitude of the first-order kernel of the input x_i for time t of the data segment at frequency f and $\bar{p}(f)$ the average of $p_t(f)$ over t at each frequency f.

2.5. Statistical analysis

The mean gain and the mean phase of the MABP and P_{ETCO_2} kernels during the entire duration of the experimental protocol in the very low (VLF; below 0.04 Hz), low (LF; 0.04–0.15 Hz), and high frequency (HF; 0.15–0.30 Hz) ranges averaged over all subjects were computed in order to further quantify the nonstationary characteristics of the estimated models and the effects of the hypercapnic step. Due to the time-varying nature of the system and the initialization of the recursive algorithm, the aforementioned quantities were expressed as mean ± standard errors based only on the last 200 s of each phase (baseline, hypercapnia and post-hypercapnia). In order to examine the effect of the hypercapnic step on the MABP phase lead, the slope (gradient) of the latter with respect to time was extracted from all subjects by applying linear regression during baseline, hypercapnia and post-hypercapnia [15]. All extracted data were analyzed using one-way ANOVA followed by Fisher's least significant procedure post hoc comparisons.

3. Results

3.1. One-input models

As it can be seen in Fig. 1a, a significant fraction of CBFV variability is explained by P_{ETCO_2}, due to the presence of the hypercapnic step. Therefore, when single-input models were used (input: MABP, output: CBFV), in order to avoid overfitting (Table 1a), the zero-order term mainly accounted for the effects of the hypercapnic step on the mean value of CBFV, as well as some slow fluctuations that were not explained by MABP (Fig. 2a and Table 1b). The corresponding time-varying linear MABP model components are shown in Fig. 3a in the time and time-frequency domains. They generally exhibit the high-pass characteristic that has been observed in previous studies [4,7], while nonstationarities are most evident in the very low frequency range (below 0.04 Hz – see also Fig. 5). The value of the forgetting factor λ_0 of the zero-order term, as selected by the genetic algorithm, was found to be small ($\lambda_0 < 0.8$) in this case (Table 1b). Furthermore, the overall model characteristics, i.e., the aforementioned high-pass frequency response of the MABP component do not appear to change as a result of the hypercapnic step.

3.2. Two-input models

In the case of two-input models, the forgetting factors for the two inputs (MABP and P_{ETCO_2}) were updated in an adaptive fashion using Cook's Distance, as described in Section 2. The decomposition of the prediction of the two-input model into its MABP, P_{ETCO_2} components is shown in Fig. 2b. It is evident that P_{ETCO_2} explains the increase of CBFV due to the hypercapnic step as well as slow CBFV fluctuations, whereas MABP accounts for fast CBFV variations, which is the expected behavior [7]. The linear time-varying kernels for MABP and P_{ETCO_2} from one representative subject are shown in Fig. 3b (top and bottom panel respectively) in the time and time-frequency domains. The general characteristics of the MABP kernels are similar to the one-input case; however, the observed nonstationarities are less pronounced (see also Fig. 5). The P_{ETCO_2} component (dynamic CO_2 reactivity) exhibits a low-pass characteristic, which has also been observed in previous studies [7]; it also exhibits a more nonstationary behavior compared to its MABP counterpart (Fig. 5). Fig. 3b (bottom panel) shows an increase in the P_{ETCO_2} kernel gain during the hypercapnic step, followed by a sharper increase at the step offset and a gradual return to its baseline values. This behavior was observed in most subjects, but the mean gain increase during hypercapnia was not found to be statistically significant (Table 2). The mean gain and the mean phase of the MABP kernels during the entire duration of the experimental protocol in the VLF, LF and HF ranges are shown in Fig. 4 averaged over all subjects. The initial baseline segment was around 10 min, but since we had to discard some samples in the beginning of the recording due to the RLS initialization, we are showing 220 s during baseline conditions.

3.3. Comparison between one-input and two-input models

Overall, one-input models exhibit more time varying characteristics and this is in accordance with recent findings regarding the presence of nonstationarities during resting conditions [18]. The forgetting factors obtained for the one-input models are smaller than those for the two-input models (Table 1b and c, respectively) suggesting more nonstationarities in the system i.e. faster or more pronounced changes in the system kernels. Moreover, comparing

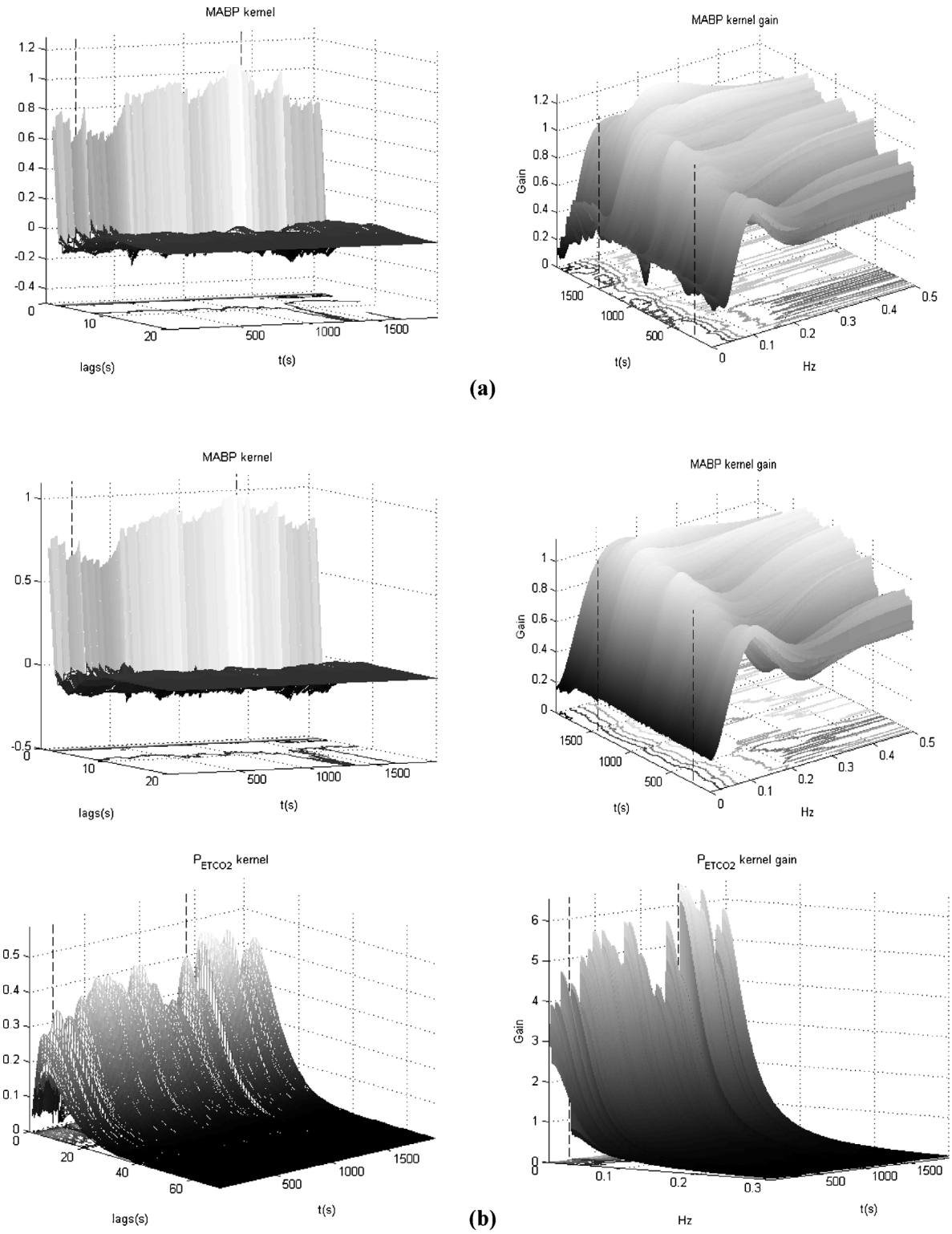

Fig. 3. Time-varying model components for one representative subject in the time (left panels) and time-frequency (right panels) domains. (a) MABP kernels for a one-input model. Nonstationarities are observed mainly in the very low frequency range (below 0.04 Hz); (b) MABP (top panels) and P_{ETCO_2} kernels (bottom panels) for a two-input model. The vertical dashed lines represent the onset and offset of the hypercapnic step. The frequency response of the dynamic pressure autoregulation component exhibits a high-pass characteristic that has been described in previous studies, which was maintained during hypercapnia.

the variability indices of the MABP kernels for the one-input and two-input models, averaged over all subjects (Fig. 5), one can see that there exist pronounced differences in the VLF range, where most of the nonstationarities are observed in all cases. This is related to the fact that P_{ETCO_2} has a significant effect on CBFV in the LF and VLF ranges. If these effects are not taken into account (i.e. a one-input model is used), the estimates of dynamic pressure autoregulation may be affected, particularly in the VLF range, where the effects of MABP and P_{ETCO_2} are both pronounced and possibly correlated.

Table 2
Mean ± standard error (the last 200 s of each experimental condition were only taken into account) of the MABP and P_{ETCO_2} kernel gain and phase estimates and of the slope of the MABP kernel phase at 1/12 Hz computed from all subjects during baseline (B), hypercapnia (H) and post-hypercapnia (PH). One-way analysis of variance and post hoc comparisons were used.

	Frequency band	B	H	PH
Mean MABP kernel phase ± SE (deg)	1/12 Hz	27.838 ± 9.258	21.249 ± 8.438*	34.091 ± 8.934*
	VLF (0.01–0.04 Hz)	75.585 ± 35.147	70.413 ± 31.676	79.697 ± 33.513
	LF (0.04–0.15 Hz)	25.290 ± 7.736	19.292 ± 8.027*	31.430 ± 8.445*
	HF (0.15–0.3 Hz)	8.091 ± 11.253	5.200 ± 12.914	4.998 ± 13.195
Mean MABP kernel gain ± SE	VLF (0.01–0.04 Hz)	0.436 ± 0.072	0.425 ± 0.067	0.372 ± 0.065
	LF (0.04–0.15 Hz)	0.752 ± 0.092	0.736 ± 0.097	0.685 ± 0.095
	HF (0.15–0.3 Hz)	0.680 ± 0.101	0.643 ± 0.121	0.690 ± 0.119
Mean P_{ETCO_2} kernel gain ± SE	VLF (0.01–0.04 Hz)	1.205 ± 0.123	1.442 ± 0.132	1.672 ± 0.204
	LF (0.04–0.15 Hz)	0.214 ± 0.029	0.258 ± 0.036	0.302 ± 0.049
	HF (0.15–0.3 Hz)	0.031 ± 0.004	0.037 ± 0.006	0.044 ± 0.007
MABP kernel phase slope ± SE (deg/s)	1/12 Hz	0.006 ± 0.002□,◊	−0.005 ± 0.002*,□ (overall)	0.0293 ± 0.006◊,*
			−0.014 ± 0.010 (during the first 2 min) / −0.004 ± 0.002 (during the rest 18 min)	

□ $p < 0.05$ B vs H.
◊ $p < 0.05$ B vs PH.
* $p < 0.05$ H vs PH.

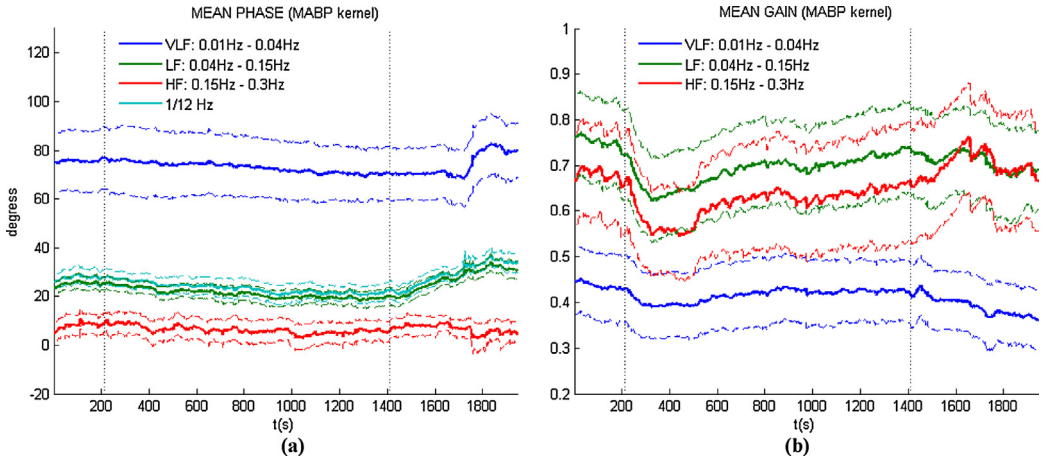

Fig. 4. Averaged (solid line ± standard error of the mean – dashed lines) (a) mean phase and (b) mean gain of the MABP kernels (right panel) for two-input models over all subjects as a function of time during the three experimental phases (baseline, hypercapnia and post-hypercapnia, where the two vertical lines denote the start and end of the hypercapnic step) in the three frequency ranges of interest (VLF: below 0.04 Hz, LF: 0.04–0.15 Hz, HF: 0.15–0.30 Hz). The cyan line in the left panel corresponds to the phase at 1/12 Hz as reported in Ref. [15].

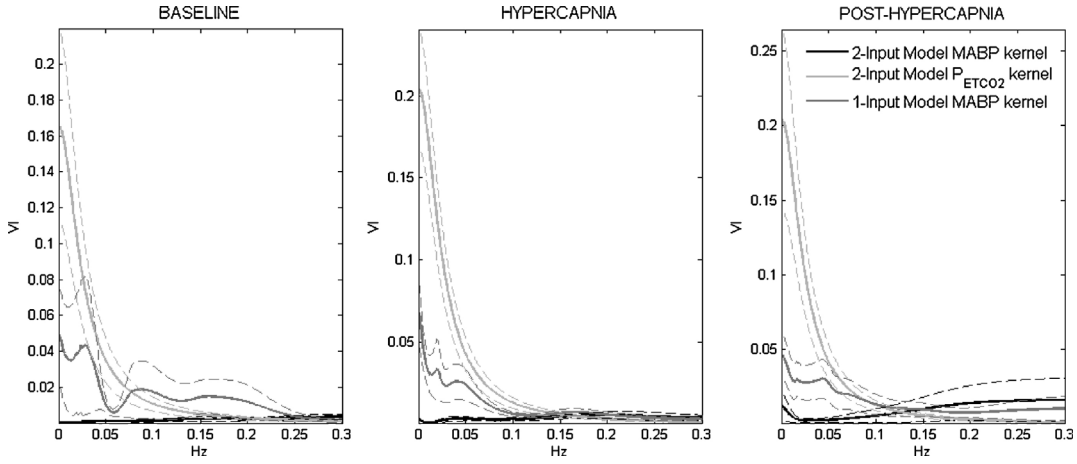

Fig. 5. Variability indices of the MABP kernels as a function of frequency for one-input and two-input models during baseline, hypercapnia and post-hypercapnia. A pronounced difference exists in the VLF range, whereby two-input models yielded considerably less nonstationary estimates for the dynamic autoregulation model component, suggesting the influence of P_{ETCO_2} in this frequency range.

4. Discussion and conclusions

We have employed a data-driven multivariate recursive approach to investigate the time-varying characteristics of cerebral autoregulation during externally induced hypercapnic steps. Data-driven approaches are well suited to the complexity of physiological systems because they yield rigorous mathematical descriptions of their dynamic behavior by utilizing input–output data, without requiring any a priori assumptions about system structure. Specifically, we examined cerebral hemodynamics in pre-menopausal women during resting and hypercapnic conditions by utilizing a two-input linear adaptive model and long duration experimental measurements of MABP, P_{ETCO_2} and CBFV.

The model parameters were updated using a recursive least squares scheme with multiple forgetting factors in order to capture the time varying characteristics of cerebral hemodynamics during experimental conditions that include a sharp transient change induced by the hypercapnic step. We experimented with both constant and adaptive forgetting factors, and we concluded that adaptive data-driven forgetting factors resulted into smoother parameter updates. This is possibly related to the fact that nonstationarities of two different kinds are expected in the present case: in addition to the fast transient changes induced by the hypercapnic step, slower time-varying changes such as those observed during resting conditions [18] are also present. Therefore, smaller values for the forgetting factors may be more appropriate around the onset and end of the hypercapnic step, whereas larger values may be more appropriate for the remaining data segments. Overall, the forgetting factor for the MABP coefficients exhibited fewer variations than the one corresponding to P_{ETCO_2} as the latter is the variable that is manipulated during the hypercapnic step.

Important features of the obtained time-varying dynamic pressure autoregulation components of the system (mean gain, mean phase) were quantified in the VLF, LF and HF ranges in order to track their time-varying characteristics during the entire duration of the recordings. No significant changes were observed for the mean gain during the latter phase (last 200 s) of the three experimental conditions (baseline, hypercapnia and post-hypercapnia – Fig. 4b). However, note the sharper decrease in the HF and LF mean gain immediately after the onset of the hypercapnic step, which gradually returns to its baseline values. Generally, the effects of hypercapnia on the mean MABP kernel gain estimates were found to be subject-specific; some settled to increased values while others to decreased values in the LF and HF ranges. Mean ± standard errors as well as the slope of the MABP phase lead with respect to time were estimated during baseline, hypercapnia and post-hypercapnia as described above. A significantly increasing trend in the MABP kernel mean phase (compared to baseline and hypercapnia), which was more pronounced in the LF range, was observed in the post-hypercapnic phase (Table 2). Importantly, the changes induced to the MABP phase lead were found to be significantly slower during the onset of the hypercapnic step than during the offset, i.e. the slope of the phase lead decrease during hypercapnia was smaller than the slope of the phase lead increase during post-hypercapnia. The calculated slope (regression coefficient) between phase lead and time was found to be statistically significant (i.e. different than zero) in all subjects ($p < 0.05$) in the LF and VLF ranges during hypercapnia and post-hypercapnia. On the other hand, the calculated slope during baseline was not statistically different than zero in most subjects and it exhibited variable behavior (positive/negative).

The above are in accordance with the results of Liu et al. [15], where the relationship between MABP and CBFV during stepwise changes of Pa_{CO_2} was identified using adaptive filters. They observed a decrease in the phase lead of the system in the LF range (1/12 Hz). Therefore, we also provide the phase for the MABP component at this particular frequency for comparison purposes (Fig. 4a). The overall observed effects of hypercapnia are similar, i.e. the reduced phase lead remains approximately constant after the first few minutes of the induced step. The negative slope values reported by Liu et al. are larger than the ones presented here (Table 2). This may be due to several different factors. First of all, the experimental protocol followed in our case was different than the one described in Ref. [15]. The duration of the hypercapnic stimulus was 20 min (as compared to 2 min in Ref. [15]), mean P_{ETCO_2} was held 8 mmHg above resting levels (as compared to 10 mmHg in [15]) and dynamic end-tidal forcing was used to control arterial gas tensions. Due to these, we computed the slope of the phase lead during the first 2 and the remaining 18 min of the hypercapnic period (Table 2). The phase drops more quickly (around three times faster) at the onset of the hypercapnic step and decreases more slowly afterwards (i.e. it appears that the slope gradually returns toward zero). This may suggest that the cerebrovascular system progressively adapts to the hypercapnic stimulus. Importantly, our modeling approach is based on a two-input model, as compared to the one-input approach used in Ref. [15] and we used multiple and adaptive forgetting factors; possibly as a result of these, we did not observe a similarly high variability for the phase lead values with respect to time as shown in Fig. 4 in Ref. [15] for subjects with lower spontaneous MABP variability.

The variability indices computed for both the MABP and P_{ETCO_2} kernels separately for each phase (Fig. 5), exhibited frequency dependencies especially in the VLF range. By comparing one-input (MABP) and two-input (MABP and P_{ETCO_2}) models, our results suggest that incorporating P_{ETCO_2} as an additional input reduces the nonstationarity of the estimates obtained by single-input (MABP–CBFV) models, suggesting the important role of P_{ETCO_2} and the possible shortcomings of assessing dynamic autoregulation using such models. In order to further illustrate the effect of P_{ETCO_2} and in order to examine whether its effects are correlated to the effects of MABP we also computed the variability indices of the MABP kernels for the two-input models, by requiring the covariance matrix $\boldsymbol{P}$ to be strictly diagonal, which suggests that the MABP and P_{ETCO_2} model parameters (i.e. the corresponding expansion coefficients) are considered independent of each other. Whereas the nonstationarity estimates are lower compared to one-input models, they are higher than the case where the covariance matrix is non-diagonal, i.e. the parameters are correlated, suggesting that the effects of correlations between MABP and P_{ETCO_2} in the VLF range could be significant. The optimized model orders and forgetting factors in this case can be found in Table 1d. The spectral estimates though for both cases (non-diagonal and diagonal $\boldsymbol{P}$) in the LF and HF range do not differ dramatically (not shown separately).

The use of CBFV as an index for CBF has been discussed extensively. CBFV changes reflect CBF changes if the cross-sectional area of the insonated vessel remains relatively constant [25]. It has been found that the diameter of the middle cerebral artery does not change in humans during moderate lower body negative pressure (up to −40 mmHg) or changes in P_{ETCO_2} [26]. Therefore, we assumed that beat-to-beat MCAV changes were a good index of beat-to-beat CBF changes. The reliability of the Finapres technique for measuring changes in arterial blood pressure has also been established [27]. Finally, variations of P_{ETCO_2} have been found to be a good index of Pa_{CO_2} variations under resting conditions [28].

In conclusion, the results suggest that nonstationarities are present in cerebral hemodynamics and that the effect of P_{ETCO_2} is significant in this context as well, as not including it as an input variable results in more nonstationary estimates for dynamic autoregulation. In the future, we aim to investigate the effect of nonlinearities by employing nonlinear models and examine their possible relation to model nonstationarities.

Competing interests

None declared.

Funding

None.

Ethical approval

The subjects gave informed consent to participate in this study, which was approved by the University of Calgary Conjoint Health Research Ethics Board.

References

[1] Panerai RB. Cerebral autoregulation: from models to clinical applications. Cardiovasc Eng 2008;8:42–59.
[2] Czosnyka M, Brady K, Reinhard M, Smielewski P, a Steiner L. Monitoring of cerebrovascular autoregulation: facts, myths, and missing links. Neurocrit Care 2009;10(3):373–86.
[3] Aaslid R, Markwalder T, Nornes H. Noninvasive transcranial Doppler ultrasound recording of flow velocity in basal cerebral arteries. J Neurosurg 1982;57:769–74.
[4] Zhang R, Zuckerman JH, Giller CA, Levine BD. Transfer function analysis of dynamic cerebral autoregulation in humans. Am J Physiol Heart Circulat Physiol 1998;274(1):H233–41.
[5] Panerai RB, Dawson SL, Potter JF. Linear and nonlinear analysis of human dynamic cerebral autoregulation. Am J Physiol Heart Circulat Physiol 1999;277(3):H1089–99.
[6] Mitsis GD, Zhang R, Levine BD, Marmarelis VZ. Modeling of nonlinear systems with fast and slow dynamics. II. Application to cerebral autoregulation. Ann Biomed Eng 2002;30:555–65.
[7] Mitsis GD, Poulin MJ, Robbins PA, Marmarelis VZ. Nonlinear modeling of the dynamic effects of arterial pressure and CO_2 variations on cerebral blood flow in healthy humans. IEEE Trans Biomed Eng 2004;51(11):1932–43.
[8] Wise RG, Ide K, Poulin MJ, Tracey I. Resting fluctuations in arterial carbon dioxide induce significant low frequency variations in BOLD signal. Neuroimage 2004;21:1652–64.
[9] Panerai RB, Simpson DM, Deverson ST, Mahony P, Hayes P, Evans DH. Multivariate dynamic analysis of cerebral blood flow regulation in humans. IEEE Trans Biomed Eng 2000;47:419–21.
[10] Mitsis GD, Zhang R, Levine BD, Marmarelis VZ. Cerebral hemodynamics during orthostatic stress assessed by nonlinear modeling regulation of the cerebral circulation cerebral hemodynamics during orthostatic stress assessed by nonlinear modeling. J Appl Physiol 2006:354–66.
[11] Mitsis GD, Zhang R, Levine BD, Tzanalaridou E, Katritsis DG, Marmarelis VZ. Autonomic neural control of cerebral hemodynamics. IEEE Eng Med Biol Mag 2009;28(6):54–62.
[12] Panerai RB, Eames P, Potter JF. Variability of time domain indices of dynamic cerebral autoregulation. Physiol Measure 2003;24.
[13] Latka M, Turalska M, Glaubic-Latka M, Kolodziej W, Latka D, West BJ. Phase dynamics in cerebral autoregulation. Am J Physiol Heart Circulat Physiol 2005;289:H2272–9.
[14] Peng T, Rowley A, Ainslie P, Poulin M, Payne S. Wavelet phase synchronization analysis of cerebral blood flow autoregulation. IEEE Trans Biomed Eng 2010;57(4):960–8.
[15] Liu J, Simpson MD, Yan J, Allen R. Tracking time-varying cerebral autoregulation in response to changes in respiratory Pa_{CO_2}. Physiol Measure 2010;31(10):1291–307.
[16] Kastrup A, Thomas C, Hartmann C, Schabet M. Sex dependency of cerebrovascular CO_2 reactivity in normal subjects. Stroke 1997;28:2353–6.
[17] Orshal JM, Khalil RA. Gender, sex hormones, and vascular tone. Am J Physiol 2004;286:R233–49.
[18] Markou MM, Poulin MJ, Mitsis GD. Nonstationary analysis of cerebral hemodynamics using recursively estimated multiple-input nonlinear models. In: CDC-ECE 2011. 2011. p. 5768–73.
[19] Marmarelis VZ. Nonlinear dynamic modeling of physiological systems. Piscataway, NJ: Wiley-Interscience & IEEE Press; 2004.
[20] Marmarelis VZ. Identification of nonlinear biological systems using Laguerre expansions of kernels. Ann Biomed Eng 1993;21:573–89.
[21] Soderstrom T, Stoica P. System identification. Englewood Cliffs, NJ: Prentice Hall; 2001.
[22] Yoshitani N, Hasegawa A. Model-based control of strip temperature for the heating furnace in continuous annealing. IEEE Trans Control Syst 1998;6(2):146.
[23] Sánchez I. Recursive estimation of dynamic models using Cook's distance, with application to wind energy forecast. Technometrics 2006;48(1):61–73.
[24] Vahidi A, Stefanopoulou A, Peng H. Recursive least squares with forgetting for online estimation of vehicle mass and road grade: theory and experiments. Vehicle Syst Dyn 2005;43(1):31–55.
[25] Poulin MJ, Robbins PA. Indexes of flow and cross-sectional area in the middle cerebral artery using Doppler ultrasound during hypoxia and hypercapnia in humans. Stroke 1996:2244–50.
[26] Serrador JM, Picot PA, Rutt BK, Shoemaker JK, Bondar RL. MRI measures of middle cerebral artery diameter in conscious humans during simulated orthostasis. Stroke 2000;31:1672–8.
[27] Imholz BP, Settels JJ, van der Meiraker AH, Wesseling KH, Wieling W. Non-invasive continuous finger blood pressure measurement during orthostatic stress compared with intra-arterial pressure. Cerebrovasc Res 1990;24:214–21.
[28] Robbins PA, Conway J, Cunningham DA, Khamnei S, Patterson DJ. A comparison of indirect methods for continuous estimation of arterial P_{CO_2} in men. J Appl Physiol 1990;68:1727–31.
[29] Panerai RB, Dineen NE, Brodie FG, Robinson TG. Spontaneous fluctuations in cerebral blood flow regulation: contribution of Pa_{CO_2}. J Appl Physiol 2010;109(6):1860–8.
[30] Dineen NE, Brodie FG, Robinson TG, Panerai RB. Continuous estimates of dynamic cerebral autoregulation during transient hypocapnia and hypercapnia. J Appl Physiol 2010;108(3):604–13.